

# Cell segregation via differential collision modes between heterotypic cell populations

Stephani Edwina Lucia<sup>†</sup>, Hyuntae Jeong<sup>†</sup>, and Jennifer H. Shin<sup>\*</sup>

Department of Mechanical Engineering, Korea Advanced Institute of Science and Technology, Seoul 34141, Republic of Korea

**ABSTRACT** In tissue development and regeneration, the establishment of sharp boundaries between heterotypic cells is essential for the differentiation of tissue functions. During the dynamic rearrangements of constituent cells that result from cell division and collective migration, the segregation boundary encounters various challenges. Several studies have suggested that cortical actomyosin structures play a crucial role in the maintenance of the boundary interface of segregated cell populations, implicating actin-mediated stresses. Examining physical cellular properties such as motility, traction, and intercellular stress, we investigated the formation and maintenance of the stable segregation between epithelial and mesenchymal cell populations devoid of heterotypic adhesions. At the contact boundary, the homotypic adhesion-mediated epithelial aggregates exerted collision-mediated compression against the surrounding mesenchymal cells. Our results demonstrated that heterotypic cell populations established a robust interfacial boundary by accumulating stress from active collisions and repulsions between two dissimilar cell types. Furthermore, the moment of the heterotypic collisions was identified by the existence of a sharp rise in maximum shear stress within the cell cluster.

## Monitoring Editor

Valerie Marie Weaver  
University of California,  
San Francisco

Received: Mar 17, 2022

Revised: Sep 12, 2022

Accepted: Sep 15, 2022

## INTRODUCTION

The importance of cell segregation during embryonic development has been emphasized (Salazar-Ciudad *et al.*, 2003; Krens and Heisenberg, 2011). During the segregation process, intercellular communication determines whether cells encounter homotypic or heterotypic cells (Fagotto, 2014; Taylor *et al.*, 2017). Consequently, the critical factor that drives the sorting is the immediate cellular

responses following the cell–cell collision, specifically the adhesion of homotypic cells to form clusters or repulsion and dispersion of heterotypic cells. In 1955, Townes and Holtfreter conducted experiments with amphibian embryos in which they mixed presumptive epidermal cells and neural plate cells and observed the sorting of the mixed cells according to their respective types (Townes and Holtfreter, 1955). Strikingly, the sorting was done in their typical configurations of an embryo, with the epidermal cells on the outside and the mesodermal cells in the middle. On the basis of these findings, cell type–specific selective affinities were proposed. Motivated by these pioneering research findings, differential adhesion, interfacial tension, high heterotypic interfacial tension, Eph/ephrin-induced repulsion, and cadherin-based readhesion at the boundary were proposed as an underlying mechanism for cell sorting. The differential adhesion hypothesis (DAH) proposed that cell segregation occurred due to the varying intercellular adhesive strengths of different cell types (Steinberg, 1970, 2007). Here, the tissue was treated as liquid with an interface, where surface tension at the heterotypic contact determined the shape of segregation. The differential interfacial tension hypothesis (DITH) model appeared as an updated alternative to the DAH model, which accounted for the contractility of the actomyosin-based cell cortex (Brodland, 2002; Amack and Manning, 2012). In the DITH model, the contact tension at the interface was established by the differential contractility and

This article was published online ahead of print in MBoC in Press (<http://www.molbiolcell.org/cgi/doi/10.1091/mbc.E22-03-0097>) on September 21, 2022.

Conflict of interest: The authors declare no competing financial interest.

<sup>†</sup>These authors contributed equally to this work.

Author contributions: S.E.L. and H. J. performed the experiment. S.E.L., H. J., and J.H.S. analyzed and discussed the data. Finally, S.E.L., H. J., and J.H.S. wrote the paper.

\*Address correspondence to: Jennifer H. Shin ([j\\_shin@kaist.ac.kr](mailto:j_shin@kaist.ac.kr)).

Abbreviations used: BSA, bovine serum albumin; DAH, differential adhesion hypothesis; DITH, differential interfacial tension hypothesis; FAK, focal adhesion kinase; HIT, high heterotypic interfacial tension; MDCK, Madin-Darby canine kidney; MSM, monolayer stress microscopy; PA, polyacrylamide; PBS, phosphate-buffered saline; ROI, region of interest; TFM, traction force microscopy.

© 2022 Lucia, Jeong, and Shin. This article is distributed by The American Society for Cell Biology under license from the author(s). Two months after publication it is available to the public under an Attribution–Noncommercial–Share Alike 4.0 International Creative Commons License (<http://creativecommons.org/licenses/by-nc-sa/4.0>).

“ASCB®,” “The American Society for Cell Biology®,” and “Molecular Biology of the Cell®” are registered trademarks of The American Society for Cell Biology.

adhesiveness, resulting in segregation. While these DAH/DITH models accurately represented the self-organization of heterotypic cell populations within the tissue, a more recent high heterotypic interfacial tension (HIT) model was able to more accurately capture the formation of higher interfacial tension through the repulsive reaction between heterotypic cells, establishing the clear and stable interface at the segregation boundary (Canty *et al.*, 2017; Fagotto, 2020). In particular, Eph/ephrin signaling at the cell surface membrane was shown to be responsible for the segregation of mixed cell types via stimulating actomyosin contraction (O'Neill *et al.*, 2016; Taylor *et al.*, 2017; Kindberg *et al.*, 2021). Consequently, it is reasonable to anticipate that such boundary formations involve actomyosin-mediated stress accumulation.

In addition to the interfacial tension at the cell–cell contact, multiple studies have investigated the role of migratory behavior in cellular segregation (Belmonte *et al.*, 2008; Kabla, 2012; Méhes *et al.*, 2012; Yang *et al.*, 2014; Beatrice *et al.*, 2017). Assuming that cells are self-propelled particles, a mathematical model predicted that the intrinsic motility of the constituent cells would have a substantial effect on the rate and morphology of segregation (Belmonte *et al.*, 2008; Beatrice *et al.*, 2017). In vitro experiments also confirmed that the greater the collectivity of the cells, the faster the segregating speed; the greater the persistence of the cell migration, the larger the segregated cluster size (Méhes *et al.*, 2012). These results confirmed that the critical role of cellular motility was the determining factor in the segregation of multiple cells in a mixed population. Nonetheless, these fine works on the role of cellular motility in segregation assumed the cell–cell interaction to be a DAH model with an intermediate heterotypic contact (Belmonte *et al.*, 2008). However, this model failed to account for the circumstance in which actively colliding cells generate a high contact tension at the heterotypic interface with almost no adhesion in between. Here, we posited the existence of collision-induced stress accumulations along the heterotypic boundary interface. By analyzing key physical properties such as migration, traction force, and intercellular stresses, we were able to track how the collective motions lead to intercellular collision events, which ultimately form the segregation boundary.

In the present study, the physical characteristics of two coculture combinations, HaCaT (epithelial type)–C2C12 (mesenchymal type) and Madin–Darby canine kidney (MDCK) (epithelial type)–C2C12 (mesenchymal type), were compared. The motile characteristics of the selected epithelial cells, HaCaT versus MDCK, were dissimilar, resulting in distinct collective motions that led to distinct segregation patterns. Nevertheless, the two pairs shared a common characteristic in which the epithelial cells were clustered as islands surrounded by the network-like C2C12 cells. Once the layout has been established, however, each pair experiences differential changes in the size and shape of the segregation pattern according to the distinct migratory behaviors of the epithelial clusters. To determine the origin of the disparity, we measured the physical basis for the segregation by employing tools to measure traction force and intercellular stresses (Trepatt *et al.*, 2009; Notbohm *et al.*, 2016; Cho *et al.*, 2018; Kwon *et al.*, 2021). Using these stress visualization techniques, namely traction force microscopy (TFM) and monolayer stress microscopy (MSM), collision-mediated stress accumulation at the heterotypic interface was identified as the most important factor in the formation and maintenance of the segregation boundary. Intriguingly, the moment of the heterotypic collisions in the cell monolayer was indicated by a sharp rise in the maximum shear stress.

## RESULTS

### Differential segregation characteristics reflect distinct collective migratory behavior of constituent cells

The formation and maintenance of segregation patterns in mixed cell populations require intimate intercellular interactions between homotypic and heterotypic cells, as evidenced by cell type-specific collective cell migration behaviors (Méhes *et al.*, 2012). To examine the effect of migratory behavior on the segregation process, two representative epithelial cell types, HaCaT and MDCK, with inherently distinct motile characteristics, were selected. Each epithelial cell type was cocultured with mesenchymal C2C12 cells, a mouse myoblast cell line, as depicted in Figure 1A. Once the mixed cell layer reached ~90% confluency, which was approximately 6 h after seeding, the dynamic segregation process was imaged. These two cell pairs, HaCaT–C2C12 and MDCK–C2C12, were chosen because the constituent cells of each pair formed distinct segregation boundaries at the heterotypic interface (Figure 1, B and C). As shown in Figure 1, D–F, the HaCaT–C2C12 pair segregated sequentially as follows: small islands of HaCaT cells wandered around as collective entities, colliding with each other to form larger clusters, while C2C12 cells formed network-like boundaries surrounding the swirling HaCaT clusters (Figure 1, D–F; Supplemental Movie S1). During the segregation process of the MDCK–C2C12 pair, on the other hand, small clusters of MDCK cells grew in size by proliferating and merging with nearby clusters, while C2C12 cells reoriented themselves to surround the MDCK clusters. Overall, the MDCK–C2C12 pair appeared to move much less (Figure 1, G–I; Supplemental Movie S2). The apparent differences in the segregation process between the two pairs appeared to be the result of intrinsic differences in the homotypic adhesion properties of the constituent cells, their collective migratory behaviors, and the heterotypic collision events that occurred at the boundary interface.

As an inherent collective behavior of HaCaT cells, Peyret *et al.* (2019) reported that the highly confluent HaCaT cell monolayer exhibited dynamic swirling motions due to the reorientation of local cellular polarities coupled with the intercellular force transmission. As depicted in Figure 2A, we have reproduced the formation of natural eddies in the highly confluent HaCaT cell monolayer. Interestingly, these intrinsic swirling motions in the HaCaT monolayer were conserved during the segregation process of the cocultured HaCaT and C2C12 cells, where HaCaT cells exhibited continuous recirculation motions within their clusters while C2C12 cells rearranged themselves along the boundaries of the HaCaT clusters (Figure 2B; Supplemental Movie S3). MDCK cells, on the other hand, moved very little, with the exception of occasional translational migrations of dense cellular packs, represented by smaller cell sizes, toward less crowded regions (Figure 2C). When MDCK and C2C12 cells were cocultured, they formed segregation patterns similar to those of the HaCaT and C2C12 pair, with MDCK cells forming clusters surrounded by C2C12 cells. Nonetheless, the overall migration of the MDCK and C2C12 cells was significantly reduced by translational movement during active proliferation (Figure 2D; Supplemental Movie S4; Supplemental Figure S1).

In addition, the migration characteristics of each cell type in coculture conditions were also quantified by manually tracking the 25 cells, each from 25 segregated clusters (Figure 2, E–J). For this analysis, each cluster's behavior was represented by a single cell. The trajectories of HaCaT versus MDCK cells showed a clear difference between the two cell types where HaCaT cells

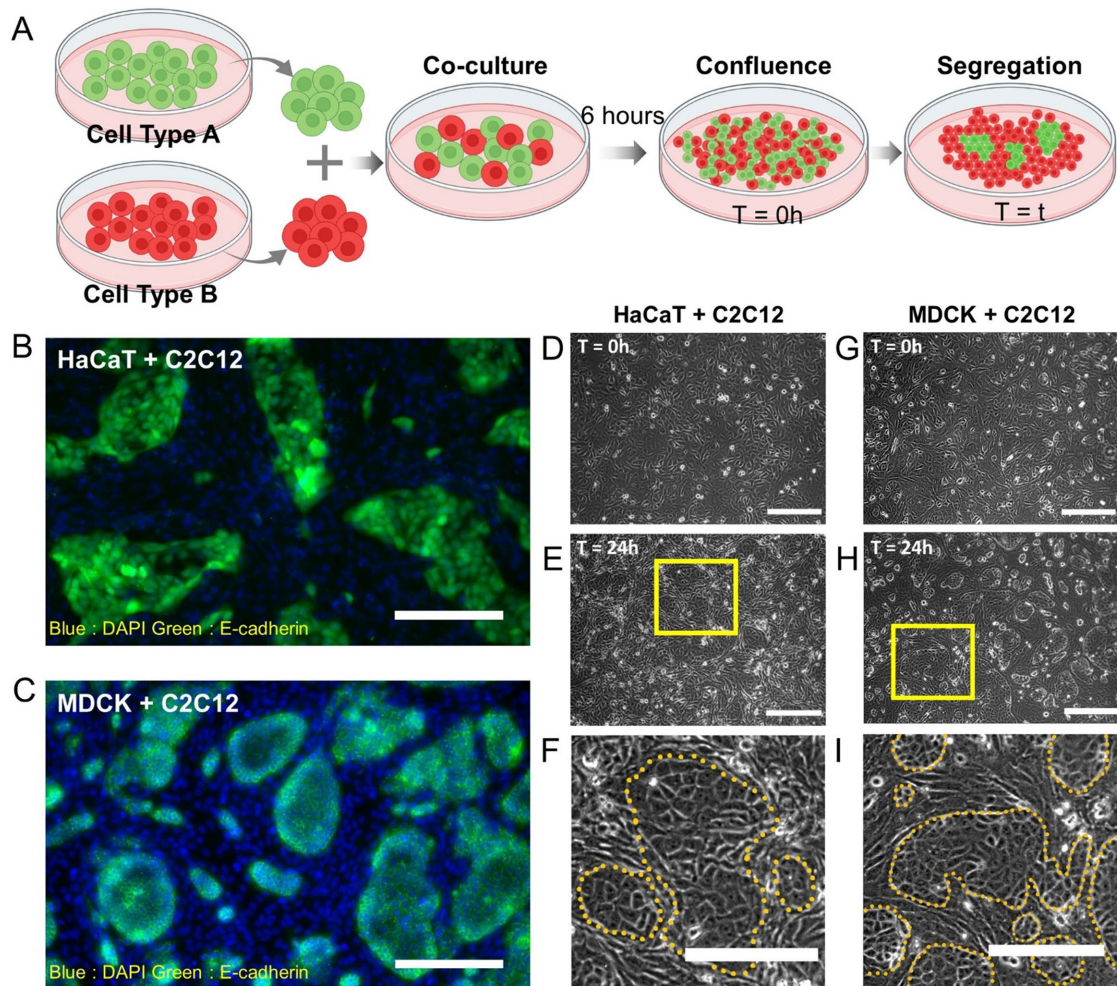


**FIGURE 1:** Formation of segregation patterns in mixed heterotypic cell populations. (A) Experimental methods of the coculture. Coculturing two cells can be done by culturing the harvested cells into the same culture dish, each with 30% confluency. This study used two distinct types of cells: epithelial (HaCaT) and mesenchymal-like (C2C12). (B, C) Immunostaining image for each coculture pair. (B) HaCaT + C2C12 pair; (C) MDCK + C2C12 pair (blue: DAPI; green: E-cadherin; scale bars: 200  $\mu\text{m}$ ). (D) Phase-contrast image of HaCaT and C2C12 cells (beginning). (E) Phase-contrast image of segregated HaCaT and C2C12 cells (after 24 h); scale bars: 300  $\mu\text{m}$ . (F) Enlargement of the cluster from the phase-contrast image; scale bars: 200  $\mu\text{m}$ . (G) Phase-contrast image of MDCK and C2C12 cells. (H) Phase-contrast image of segregated MDCK and C2C12 cells (after 24 h); scale bars: 300  $\mu\text{m}$ . (I) Enlargement of the cluster from the phase-contrast image; scale bars: 200  $\mu\text{m}$ .

exhibited superior motility compared with MDCK cells; in particular, HaCaT cells exhibited continuous directional changes during the swirling motion (Figure 2, E and F). Figure 2, G and H, illustrates that the motile phenotypes of C2C12 exhibited distinct tendencies depending on the opponent epithelial cells. During the segregation, the coculture of C2C12 cells with HaCaT cells enhanced their motile functions, such as averaged cellular speeds and directional persistence. It was most likely due to the potential existence of frequent interactions or guidance by inherently dynamic HaCaT cells (Figure 2, I and J). The migration speeds of both epithelial cell types also significantly decreased in the presence of C2C12 cells, which reflected possible influence according to the heterotypic cell interactions (Figure 2I). Taken together, the velocity fields and motile properties demonstrated that the intrinsic motile properties of each constituent cell type within the coculture dictated the overall dynamics of cell segregation.

### Segregation boundaries are formed by collision-mediated interfacial stress accumulations between heterotypic cell populations

HaCaT cells maintained robust swirling motions even after establishing segregation (Figure 3A). These swirls within the HaCaT clusters frequently migrated to the interface and collided with C2C12 cells. Following the collision, the swirling cluster of HaCaT cells abruptly changed direction. In the example shown in Figure 3, B and C, HaCaT cells exhibited the directional changes 18 h after reaching  $\sim 90\%$  confluency. The cell trajectories depicted in Figure 3D revealed that randomly migrating HaCaT cells formed collective clusters after  $t = 11$  h. As the collective entity, the rotational movement of HaCaT cells persisted as they sheared against the C2C12 cells at the boundary. To determine the moment of collision, we mapped the velocity of the cells in the region immediately adjacent to the boundary where the predominant rotational movements occurred, as marked by the white dotted line in Figure 3D. Each

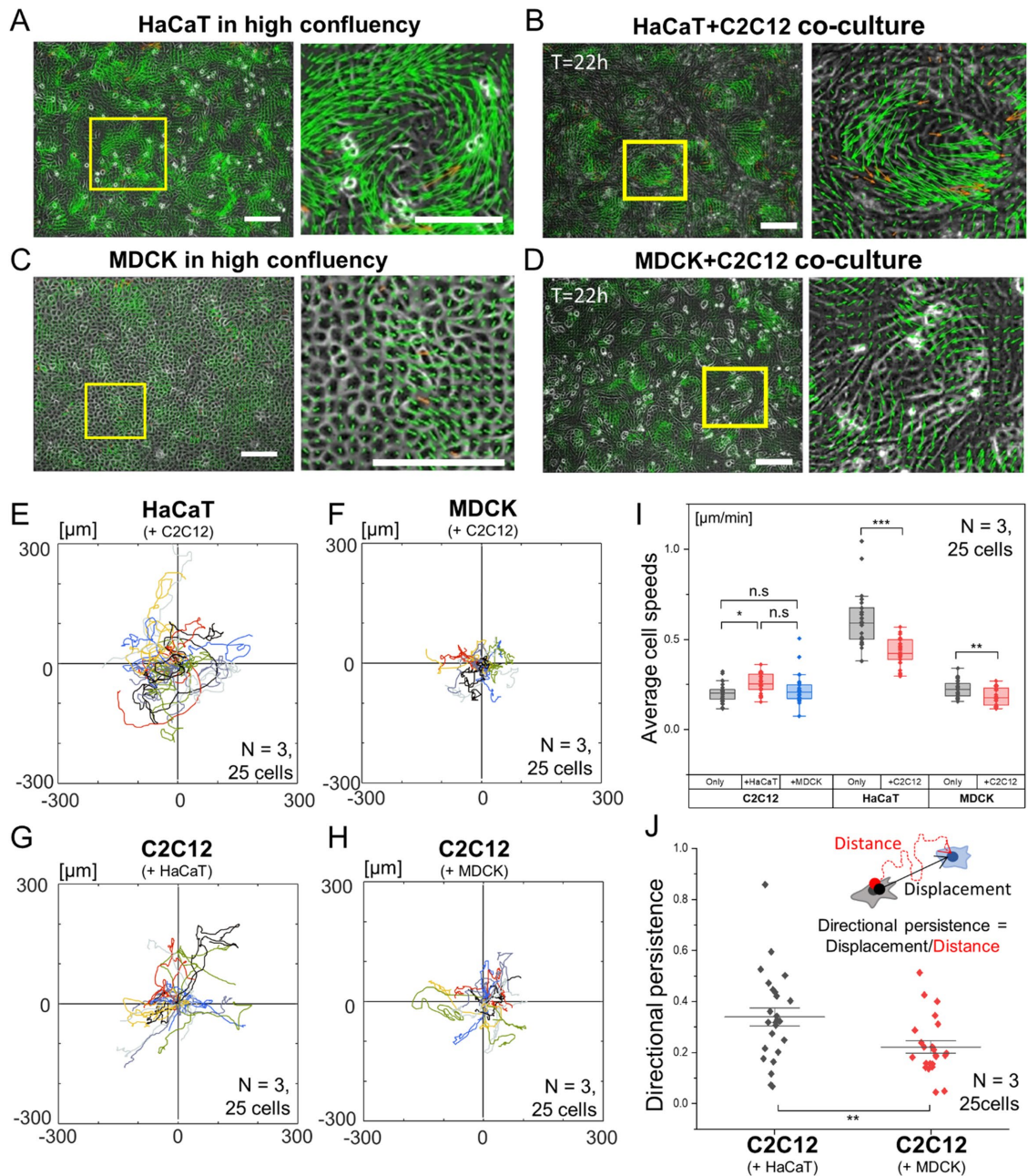


**FIGURE 2:** Migration phenotypes of various cell types in monoculture and coculture conditions. (A, B) Phase-contrast images of HaCaT in monoculture and coculture conditions with velocity vectors (green arrows); scale bar: 200  $\mu\text{m}$ . (C, D) Phase-contrast images of MDCK in monoculture and coculture conditions with velocity vectors (green arrows); scale bar: 200  $\mu\text{m}$ . (E, F) Motion trajectories of epithelial cell types in coculture condition: (E) HaCaT and (F) MDCK. (G, H) Motion trajectories of C2C12 cells in each culture state condition: (G) with HaCaT and (H) with MDCK. (I) Average cell speeds at higher cell density (24 h after confluent state) in both monoculture and coculture conditions. (J) Directionality of C2C12 in coculture conditions. \*  $p$  value < 0.05, \*\*  $p$  value < 0.01, \*\*\*  $p$  value < 0.005.

region of interest (ROI) for HaCaT and C2C12 was chosen near the colliding interface, as indicated by the yellow dotted lines, in order to selectively trace the changes of neighboring cells of the collision site from snapshot images at  $t = 12$  h, when the clear segregation boundary was formed (marked by the solid white line). Here, we spatially fixed the ROIs to focus on the temporal changes in cellular speeds and stresses near the collision site. As collisions occur continuously along the boundary, the moving ROIs following the moving interface would be incapable of capturing the changes before and after collisions. Here, we anticipated that the collision between

two heterotypic cells with negligible binding affinities would result in abrupt changes in their motile behavior. Particularly in the case of highly motile HaCaT cells with a swirling motion, cells exhibited a sliding motion against the boundary when they encountered less motile C2C12 cells, resulting in a significant change in the collective motion of HaCaT cells near the collision site. In this scenario, one can imagine that the collision events between HaCaT and C2C12 cells at the interface should result in the reversal of the normal velocity component and a relatively high tangential velocity component within the actively moving HaCaT cell cluster. The analyses of

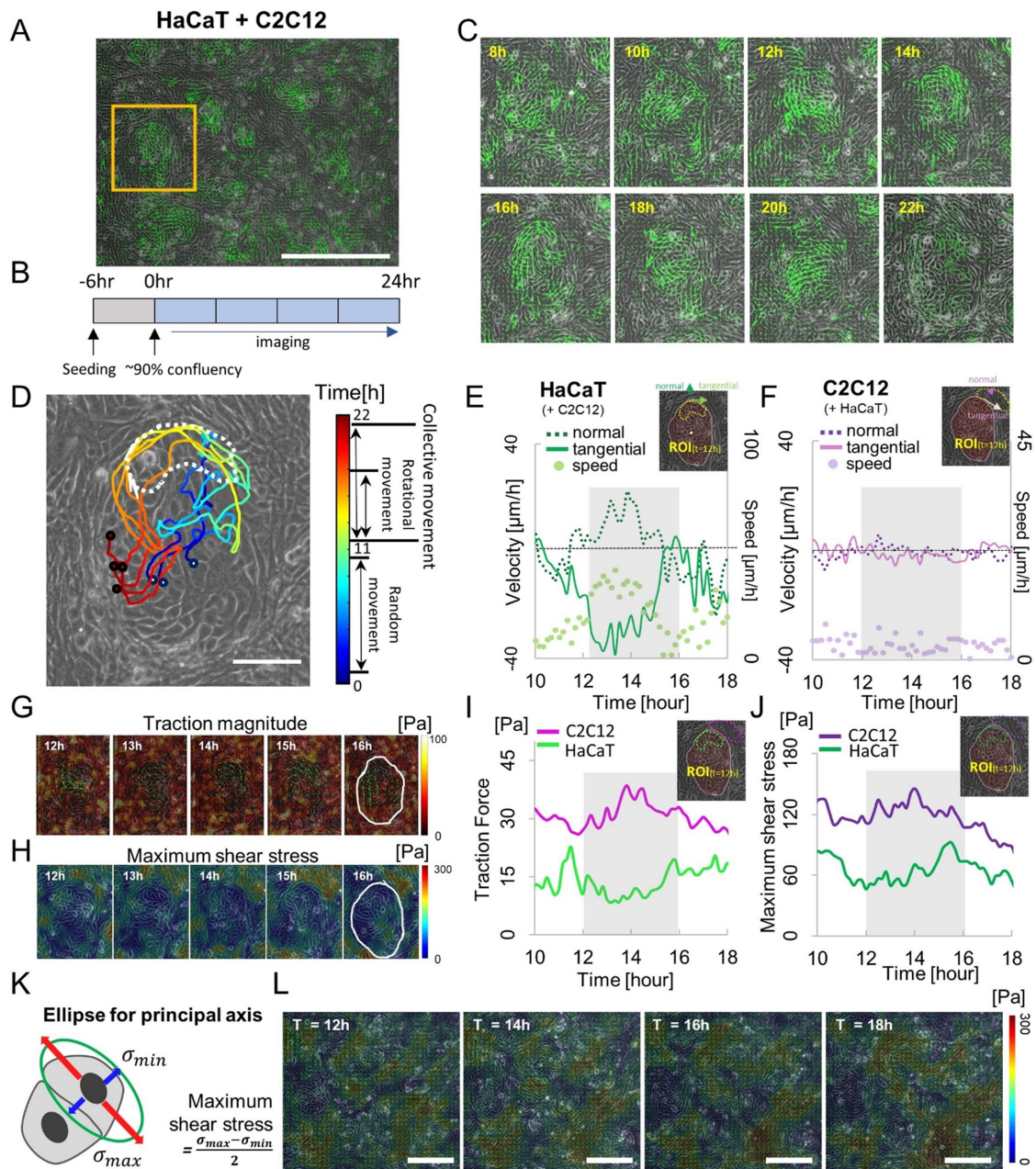


**FIGURE 3:** Changes in dynamic traits along the interfaces between HaCaT and C2C12 during the segregation. (A) Velocity vector fields during the segregation in HaCaT and C2C12 coculture condition; orange box: ROI; scale bar: 500  $\mu\text{m}$ . (B) Timetable for the experiment condition. (C) Temporal changes of velocity fields at the ROI. (D) Temporal changes of velocity fields at the ROI. (E) The trajectories of HaCaT cells inside segregated clusters, where the color of lines shows the temporal domain (white dotted line: the ROI for collision events). (F) Plots for the averaged velocity components (dotted line: normal; solid line: tangential) of cells in the ROI at the interface (yellow dotted line). The normal and tangent directions were determined by measuring the radial and circumferential direction with respect to the center point of the epithelial cluster; scale bar = 100  $\mu\text{m}$ . (G) Changes in cellular speeds of C2C12 during the segregation process at the ROI. (H, I) Visualized results of cellular traction force and maximum shear stress near the ROI. (J) Change of traction forces of two cells near the ROI. (K) Changes of maximum shear stress near the ROI. (L) Meaning of maximum shear stress inside the monolayer. (M) Sequential map of maximum shear stresses during the segregation, where the green ellipsoids indicate the ellipse of the principal axis; scale bar = 200  $\mu\text{m}$ .

velocity components within the ROI shown in Figure 3E suggested the existence of active heterotypic collisions with sliding motions between HaCaT and C2C12 during the 12–16 h time window, which eventually led to the reversal of normal motion with respect to the boundary beyond  $t = 16$  h. In contrast, no significant changes were observed in the C2C12 motility, as assessed by the changes in

velocity components and the speed within the ROI drawn in the C2C12 side of the boundary (Figure 3F). In this case, it seemed plausible to assume that the C2C12 network surrounding the HaCaT cell clusters must have resisted the collisions from HaCaT cells without surrendering their positions. This momentary resistance by C2C12 cells at the boundary would cause HaCaT cells to move

away after collisions. To further evaluate the resistance by C2C12 during the collision process, we mapped the spatiotemporal distribution of stresses in C2C12 cells within the ROI. As shown in Figure 3, G and H, the cell–substrate traction force and intercellular stress were analyzed during the segregation process. The temporal variation in the traction shown in Figure 3I suggested that C2C12 cells exerted greater traction on the substrate between 11 and 16 h, whereas the HaCaT cluster slid against the heterotypic boundary. On the other hand, for actively migrating HaCaT cells, the overall traction magnitude was smaller, and no noticeable time-dependent changes were observed (Figure 3I). The intercellular stresses were then calculated based on the force equilibrium of the traction force distributions in the cell monolayer. As shown in Supplemental Movie S5, we compared the maps of various intercellular stress components during the segregation process. The mean stress, which expresses the tensional state of cells, exhibited incoherent spatial distributions over the cocultured monolayer. The mean stress values at the boundaries of C2C12 around HaCaT clusters exhibited no discernible patterns, whereas the shear component of the stress suggested a correlation along with the segregated boundary interface between the two cell types. Specifically, the maximum shear stress was clearly elevated along the C2C12 boundary as the segregation was formed (Supplemental Movie S5; Figure 3H). Looking more closely, the maximum shear stress within the ROI of the C2C12 cells increased as the HaCaT cells approached, collided, and slid at the interface up to about the 14 h time point, followed by a gradual decrease as the pack of rotational HaCaT cells steered away (Figure 3J). Given that the maximum shear stress is the average value of the difference between the maximum and the minimum stresses along the principal axis (Figure 3K), high maximum shear stress would indicate a strong anisotropy in the intercellular stresses about the principal axis. As indicated by the principal axis map near the boundary, C2C12 cells were subject to tension in the tangential direction and compression in the normal direction (Figure 3L). In conclusion, the repulsive pressure from the collisions of HaCaT cells was shown to induce the changes in traction force and intercellular stress of the boundary cells without causing the boundary displacement.

In contrast to the swirling motions observed within the densely packed HaCaT cells, MDCK cells exhibited expansion migration toward the less crowded region (Figure 2, A and C). Even under coculture conditions with C2C12 cells, MDCK clusters surrounded by C2C12 cells exhibited a collective translational motion (Figure 4, A–C). Moreover, the MDCK packs had a more irregular shape than the HaCaT clusters (Supplemental Figure S2, A and B). Within the cluster, the trajectories of MDCK cells also exhibited limited displacements and little persistence. Nonetheless, the MDCK pack continually grew in size by expanding against the MDCK–C2C12 boundaries over the course of 22 h (Figure 4D). Here, the velocity components were tracked by setting  $t = 0$  when the monolayer reached ~90% confluency, and the ROIs were selected for both MDCK and C2C12 on the snapshot image at  $t = 12$  h when the segregation was stably established. As shown in Figure 4E, the velocity in the normal direction had positive peaks between 11 and 16 h, suggesting the radially outward movements toward the boundary within the ROI. During this time period, the values of the normal velocity component of C2C12 cells also were predominantly positive, indicating that the C2C12 cells were being radially pushed outward by the expansion of the MDCK cluster (Figure 4F). The overall speed of MDCK was much lower than that of HaCaT, and interestingly, the C2C12 cells exhibited a much slower speed when cocultured with MDCK (Figures 3, E and F, and 4, E and F). For compari-

son with the HaCaT–C2C12 pair, both traction force and maximum shear stress values were plotted and quantified, as shown in Figure 4, G–J. The collision-induced momentary boundary resistance in C2C12, previously evidenced by higher traction values in the HaCaT–C2C12 pair, was not observed in the MDCK–C2C12 pair because the increase in traction force of C2C12 was not statistically significant. Instead, gradually increased traction and maximum shear stress values in C2C12 cells persisted for some time, supporting the scenario of the heterotypic boundary being slowly pushed by the expanding MDCK while being counterbalanced by C2C12 cells at the boundary (Figure 4, I and J).

### Collision-induced resistance leads to aligned cytoskeletal bundles at the boundary interface

We then investigated the changes in the actin cytoskeleton because the bundled actin fibers are known as force-generating mechanotransducers (BurrIDGE and Wittchen, 2013). As shown in Figure 5, A and B, the HaCaT–C2C12 and MDCK–C2C12 pairs showed dissimilar actin structures. In the HaCaT–C2C12 condition, actin fibers were aligned circumferentially, forming network-like structures encircling HaCaT cell clusters (Figure 5A). These highly aligned bundles surrounding the HaCaT clusters must correspond to the physical barriers to withstand the collision-induced tension at the boundary interface. In the MDCK–C2C12 condition, however, thin actin bands were formed around the MDCK cluster boundary, whereas the actin fibers in the C2C12 network lacked obvious alignments (Figure 5B). To quantify the degree of alignment of actin fibers in C2C12 cells, we first drew a line representing the minimum distance between two clusters (solid line in Figure 5C) and set the vertical bisector of this line as the reference line. As shown in Figure 5C, we then measured the angle between actin fibers and the reference line. Actin fibers in the HaCaT–C2C12 pair exhibited predominantly clustered distributions near  $0^\circ$  and  $180^\circ$ , indicating parallel alignment of fibers to the circumferential interface, whereas the orientations of fibers in the MDCK–C2C12 pair were widely distributed. Having an aligned actin cytoskeleton is often correlated with an aligned nucleus, reflecting the alignment of cells within the monolayer. Although the nuclear sizes in C2C12 populations in both the HaCaT–C2C12 pair and the MDCK–C2C12 pair were not statistically significant, the nuclear aspect ratio was significantly greater in the HaCaT–C2C12 pair, indicating elongated nuclear shapes (Figure 5, C and D). These results suggested that the C2C12 cells were subjected to greater normal directional compression in the HaCaT–C2C12 pair than in the MDCK–C2C12 pair. Thus, we were able to relate the formation of the segregation boundary structure to the differential motile properties of the cell clusters (Figure 5E). HaCaT cells exhibited collective migration as cohesive packs that steered against the heterotypic boundary in a rotational motion, causing transient collisions. During these collisions, the interface between HaCaT and C2C12 cells was attuned and shaped to form a thick boundary by the collision-induced pressure, but the inner HaCaT cluster needed not fully fit the boundary. On the other hand, MDCK cells migrated slowly in the direction of expansion while maintaining contact between MDCK and C2C12 cells at the boundary interface. Therefore, the pressure on the C2C12 cells at the boundary was typically more homogeneous than that on the HaCaT–C2C12 pair. Conclusively, the motile characteristics of inner cells, HaCaT versus MDCK, and their contact behavior at the interface with C2C12, transient collisions versus steady push, were found to be two major factors in determining the segregation patterns of two heterotypic cell types with negligible cell–cell interactions.

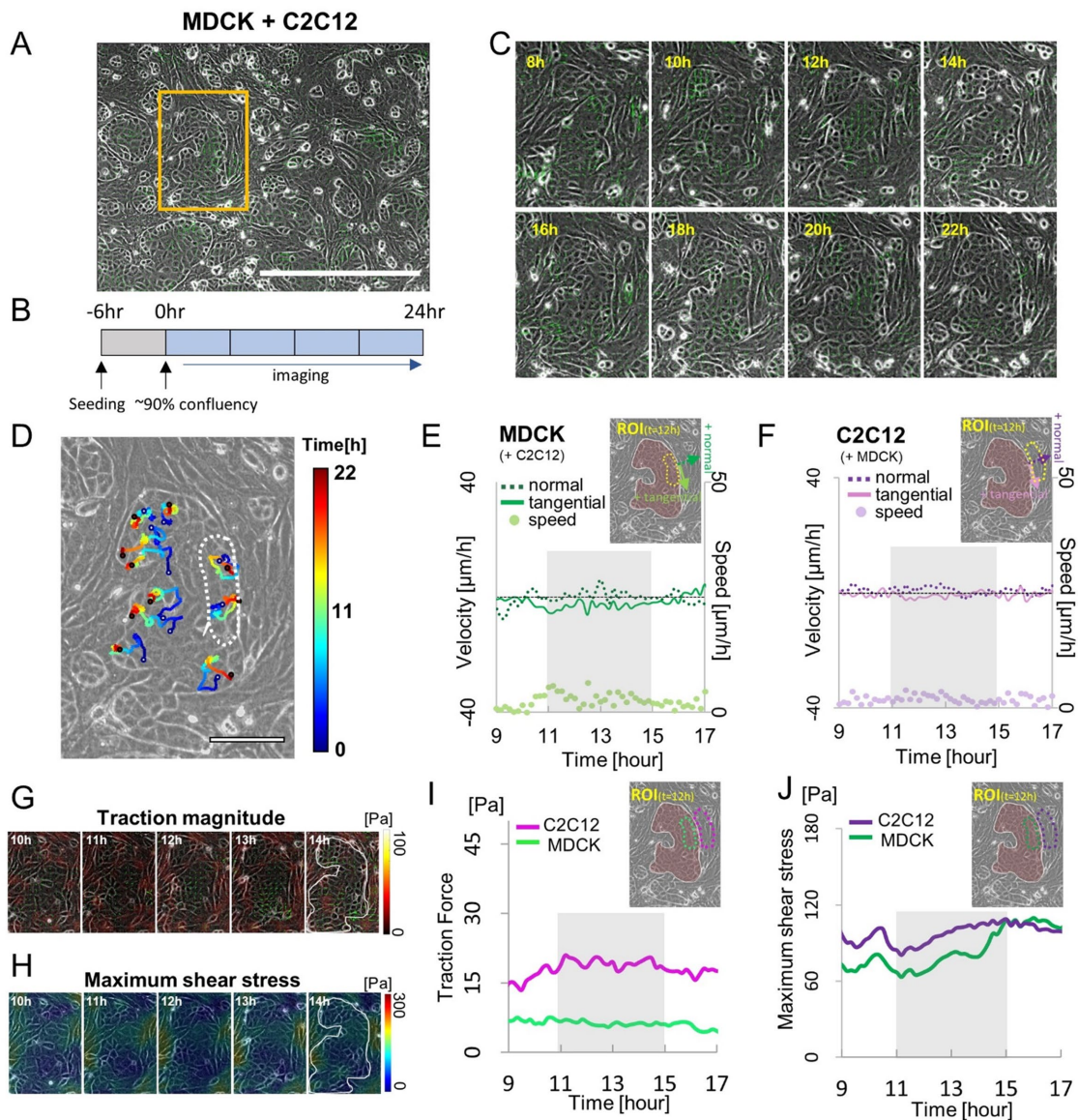


**FIGURE 4:** Changes in dynamic traits along the interfaces between MDCK and C2C12 during the segregation. (A) Velocity vector fields during the segregation in MDCK and C2C12 coculture condition; orange box: ROI; scale bar: 500  $\mu\text{m}$ . (B) Timetable for the experiment condition. (C) Temporal changes of velocity fields at the ROI. (D) The trajectories of MDCK cells inside segregated clusters, where the color of lines shows the temporal domain (white dotted line: the ROI for collision events). (E) Plots for cell velocity components (dotted line: normal; solid line: tangential) at the ROI (the region in the yellow line); the normal and tangent directions with respect to the center point of the epithelial cluster. (F) Changes in cellular speeds of C2C12 during the segregation process at the ROI (yellow line). (G, H) Visualized results of cellular traction force and maximum shear stress near the ROI. (I) Change of traction forces of two cells near the ROI. (J) Changes of maximum shear stress near the ROI.

### Myosin II plays a critical role in the maintenance of segregation boundaries between HaCaT and C2C12

Motile characteristics of inner clusters and the differential contact behavior between two heterotypic cells were crucial in establishing segregation patterns. Especially for the HaCaT–C2C12 pair, the formation of a smooth and distinct segregation boundary between these two cells appeared to be closely linked to the collision events involving highly motile HaCaT cells and the tensile resistance in the surrounding C2C12 cells. As the motility and tensile resistance were governed by actomyosin-mediated intracellular force generation, we selected a pharmacological inhibitor, blebbistatin (50  $\mu\text{M}$ ), to

suppress myosin II activities in order to investigate the role of myosin II in the maintenance of segregated patterns. In contrast to untreated control (Figure 5A), the blebbistatin-treated segregation pattern exhibited disintegrated boundary features after 24 h of treatment, which may indicate the compromised resistance by stress fiber-mediated intercellular tension (Figure 6A). To quantify the loss of the resistance of boundaries, we first waited for 18 h until the segregated patterns were established. The initial time ( $t = 0$ ) was set as the point where the mixed cells reached  $\sim 90\%$  confluency before adding blebbistatin and analyzing the temporal changes in stresses and overall morphology in segregated patterns for the first 12 h

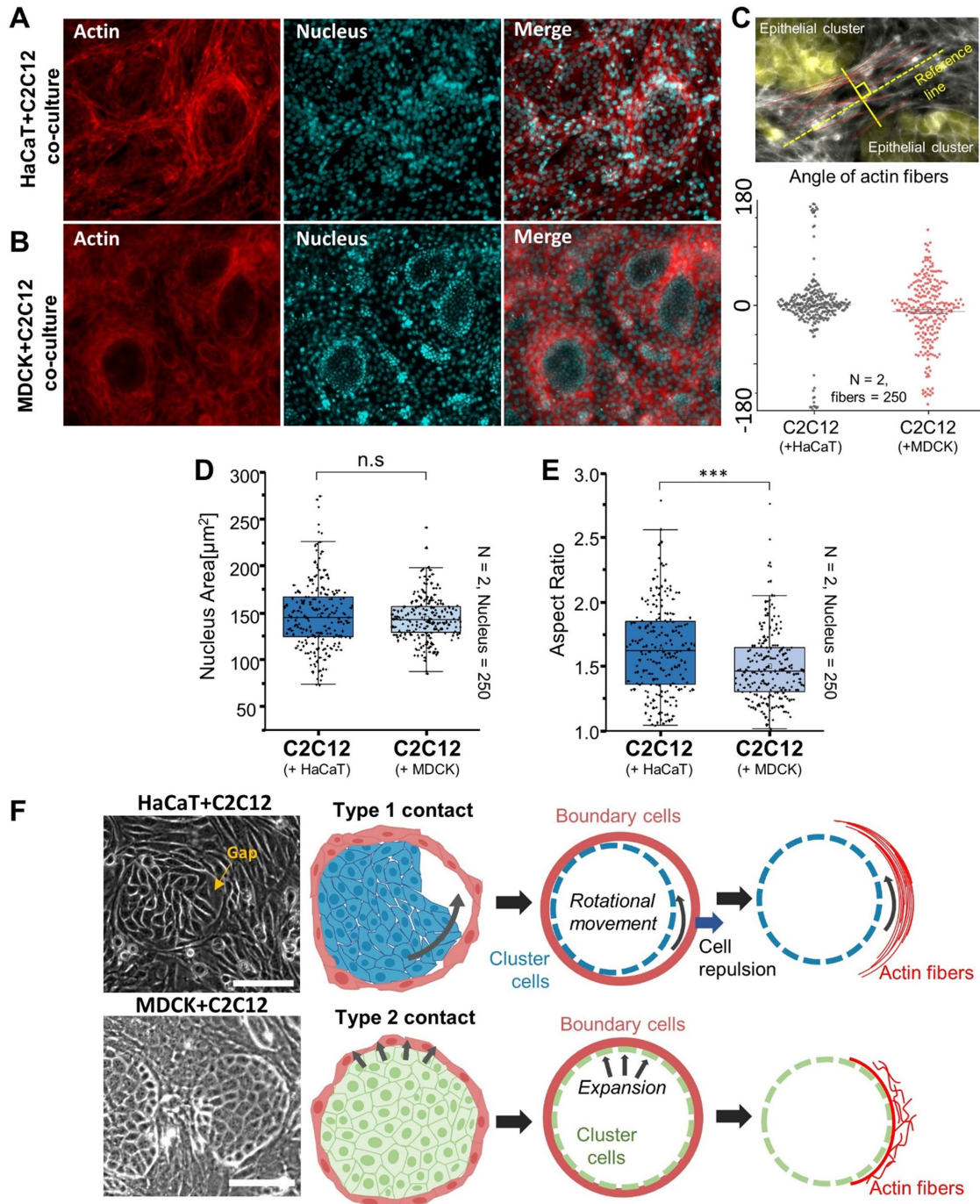


**FIGURE 5:** Collision mode-dependent differential cytoskeletal structures. (A, B) Formation of network-like actin structures around the segregated clusters in the coculture conditions: (A) HaCaT + C2C12 and (B) MDCK + C2C12; scale bar: 200  $\mu\text{m}$ . (C) Quantification of the alignment of actin fibers between adjacent segregations. (D, E) Morphological characteristics of C2C12 nucleus in the coculture conditions. (F) Schematic representation of mechanism according to the motile function of inner cells. \*\*\* $p < 0.005$ .

after blebbistatin treatment (Figure 6B). As shown in Figure 6, C and D, the suppression of myosin II significantly reduced the overall values of traction force and maximum shear stress. Specifically, initially highlighted stresses around the boundary at  $t = 0$  were diminished at  $t = 12$  h, supporting the importance of myosin II-induced force maintenance at the segregation boundary. To investigate the role of stress fiber-induced tensions in maintaining the cluster shape and boundary morphology, we quantified the changes in the irregularity

and the roughness of the cluster shape by utilizing the circularity ( $4\pi \text{Area}/\text{Perimeter}^2$ ) and solidity ( $\text{Area}/\text{Convex hull area}$ ) of the clusters, respectively (Figure 6, E–G). Circularity is a measure of how similar the shape is to a circle, taking into consideration the smoothness of the perimeter, whereas solidity measures the overall concavity of the shape. As shown in Figure 6F, the clusters maintained their smooth circular boundary in untreated control, but the circularity dropped noticeably with the blebbistatin treatment. The decrease in solidity

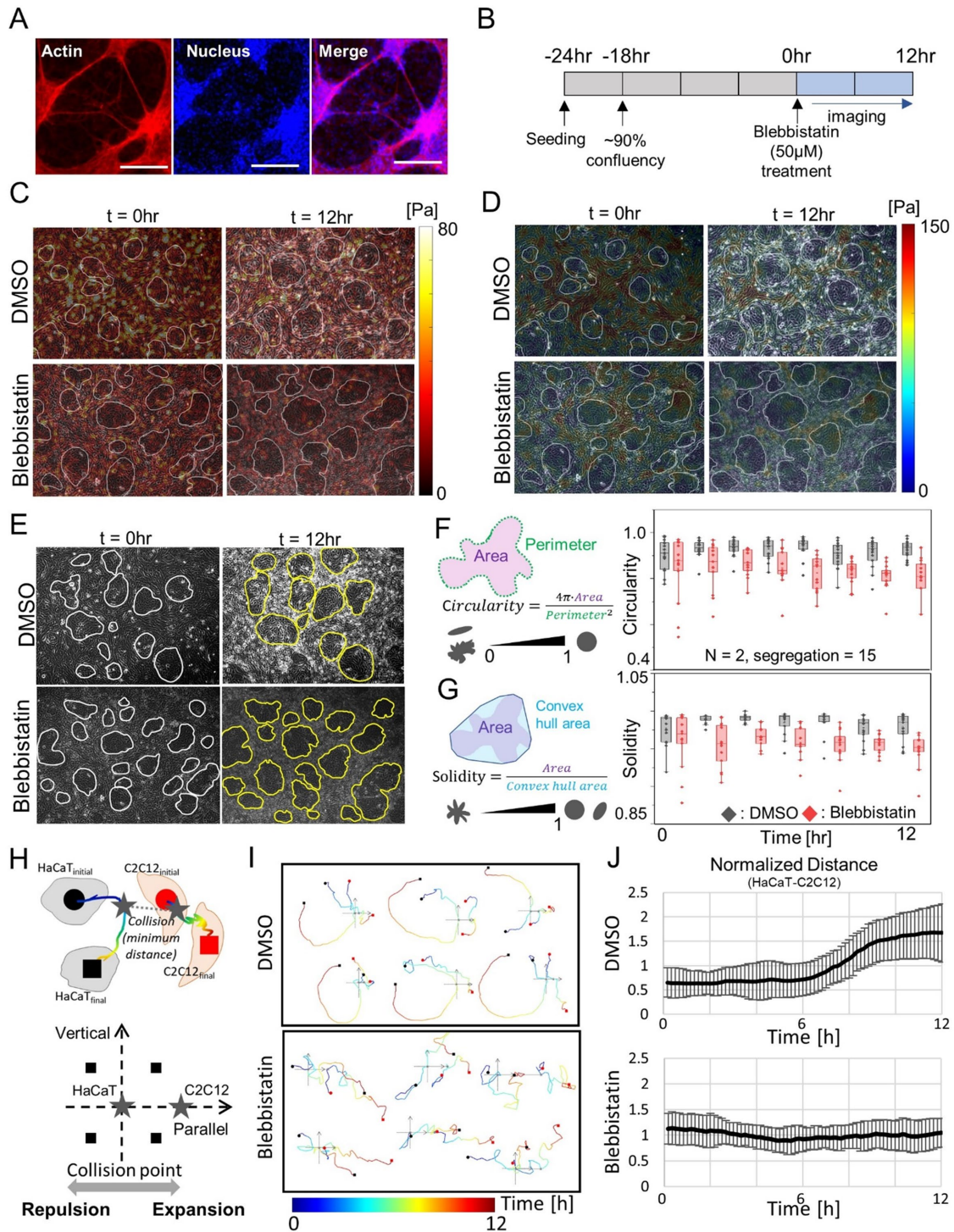


**FIGURE 6:** Elucidation of mechanisms in the collision between HaCaT and C2C12 in terms of myosin II activities. (A) Immunostained actin structures around the segregated clusters of HaCaT–C2C12 coculture conditions with blebbistatin treatments; scale bar: 200  $\mu$ m. (B) Timetable for the experiment conditions. (C, D) Changes of traction forces (C) and maximum shear stress (D) distributions in dimethyl sulfoxide and blebbistatin treatment conditions. (E) Changes of segregated patterns per blebbistatin treatment (white and yellow lines: boundaries between HaCaT and C2C12). (F) Effect of blebbistatin treatment in temporal changes in the circularity of clusters according to the chemical treatments. (G) Effect of blebbistatin treatment in temporal changes in the solidity of boundaries according to chemical treatments. (H) Schematics for collision plots and the expectation results for two types of cell movements after collision (1. Repulsion, 2. Expansion). (I) Representative trajectories of HaCaT and C2C12 during the collision event (circle: initial positions of HaCaT (black) and C2C12 (red); star: final positions of HaCaT (black) and C2C12 (red); gray line: position of minimum distance between HaCaT and C2C12). (J) Trends of normalized distance (present distance/initial distance) between HaCaT and C2C12 during the collision.

values brought about by blebbistatin also confirmed that the boundary interface had lost its integrity, resulting in a wrinkly morphology. This observation was most likely attributable to compromised intercellular actin cables across interfacial C2C12 cells. However, because blebbistatin globally inhibits myosin activity, compromising actomyosin tension at the cell–cell interface as well as cell–substrate adhesions, two additional experiments were performed to confirm the effect of myosin II. First, myosin activities were enhanced by calyculin A. When the segregated cocultured samples were treated with calyculin A, the sizes of the segregated HaCaT clusters were maintained over time. Considering that the normal segregated HaCaT clusters grew in size over 12 h by cell division and colliding migration to the C2C12 boundary, the effect of calyculin A highlights the important role of myosin II in encircling the clusters to maintain the segregation morphology (Supplemental Figure S3). Second, we also investigated the effects of the cell–substrate interaction on segregation by inhibiting the focal adhesion kinase with FAK inhibitor (FI) 14 treatments. The results indicated that the structure of the segregation pattern did not change with suppressed focal adhesion kinase (FAK), confirming that the actomyosin structure at the interface, not the cell–substrate adhesion, must play a crucial role in maintaining the segregation form. Therefore, even if blebbistatin may globally affect both cell–cell and cell–substrate junctions, the effects of blebbistatin shown in Figure 6, A–G, were still valid. Furthermore, suppression of FAK did not change segregation size despite the low cellular mobility, confirming that physical collisions caused by cell movement result in actual segregation alterations.

To further elucidate how the collision-induced tension at boundaries was affected by the suppression of myosin II activity, we investigated the cell trajectories of inner HaCaT cells and outer C2C12 cells colliding with each other during the segregation (Figure 6H). We first placed the initial locations of two cells (solid circles), one HaCaT and the other C2C12, and drew a colliding trajectory to lie on the x-axis, and the y-axis was drawn vertically from the collision point (solid gray star) between two cells. In this configuration, the final positions (solid squares) of HaCaT landing in either the second or the third quadrant would be considered repulsion after the collision, resisted by the tension cable in boundary C2C12 cells. On the other hand, the final positions on the first and fourth quadrants would indicate the persistent migration after the collision in the absence of any boundary resistance by C2C12 cells (Figure 6H). HaCaT cells in the control condition exhibited the turnaround motion after the collision, marked by gray stars, landing in the second or third quadrant (Figure 6I). However, with the suppressed myosin II activities, the HaCaT cells did not show any repulsion motion, continuing to migrate with any significant directional change to end up in either the first or the fourth quadrant (Figure 6I). Similar trajectories between HaCaT and C2C12 cells after collision in the blebbistatin-treated sample support the notion that C2C12 cells are not able to resist the colliding HaCaT cells back but instead surrender backward. The normalized distance between HaCaT and C2C12 cells shown in Figure 6J also confirmed these motile characteristics. These results supported our model in which actomyosin-mediated mechanical tensions induced by the heterotypic collective collision were proposed as the primary factor in the development and maintenance of the segregation patterns.

## DISCUSSION

Within a tissue, cells communicate via biochemical signals and physical contacts. In particular, cells in densely packed collectives interact via both homotypic cell–cell junctions and heterotypic repulsions (Mishra *et al.*, 2019). Owing to the fact that all tissues are inherently

heterogeneous, consisting of multiple cell types, it is essential to comprehend the repulsion behavior at the heterotypic contacts (Altschuler and Wu, 2010; Schumacher *et al.*, 2017). Here, we constituted the heterotypic collision modes by coculturing different cell types and investigated the mechanism of how the segregation boundary was established and maintained through the heterotypic collision-induced mechanical tensions at the boundary interface. To study distinct heterotypic contact modes, two representative epithelial cell types, HaCaT and MDCK, of inherently distinct migratory behaviors were chosen and cocultured with mesenchymal C2C12. When the trajectories of HaCaT and MDCK cells were compared, HaCaT cells exhibited superior motility compared with MDCK cells, with a prominent collective swirling motion.

Intriguingly, when cocultured with C2C12, the speed of HaCaT was significantly reduced, while the average cell speeds for C2C12 cells remained unaffected in coculture. If one could imagine a situation where two heterotypic cells were to make frequent collisions with negligible binding affinities between them, these cells would likely lose some of their potentials to move around, and the after-collision behavior would depend on the inertia of the constituent cells. Interpreting the cell speeds from the kinetic energy point of view, the dramatic decrease in HaCaT cells' speed in the coculture condition would imply the existence of direct physical collisions at the heterotypic boundary interface between HaCaT and C2C12 cells, whose inherent inertial effects were different.

With the active collisions in mind, our results confirmed that heterotypic cell populations of HaCaT–C2C12 formed a robust interfacial boundary by the collision-induced stress accumulation between two cell types. First, the traction force in the C2C12 border cells increased during the heterotypic collision, suggesting that cell–matrix anchorage must play an essential role in maintaining the boundary interface. Moreover, this very moment of the heterotypic collisions between HaCaT and C2C12 could be identified by the existence of a sharp rise in maximum shear stress within the cell cluster. The tangentially aligned principal axis of intercellular stresses and elevated maximum shear stress indicates higher mechanical tension in the tangential direction of the boundary and higher compression in the normal direction of the boundary. Per the increment of maximum shear stresses, the stress fibers also aligned along with the heterotypic contacting boundary, and the aligned boundary with tension collapsed when myosin II activities were suppressed by blebbistatin. In other words, the heterotypic collisions formed contractile actomyosin-mediated interfacial tension for a stable interface, similar to the case of the Eph/ephrin repulsion mechanism at the heterotypic contact in the HIT model. Taking all these analogies between the HIT model and our heterotypic collision model, we suggest that the locally accumulated maximum shear stress along the boundary interface must reflect the formation of interfacial tension that leads to repulsion between heterotypic cell populations. This observation was particularly intriguing because a sharp rise in maximum shear stress can be used as a measure to identify heterotypic collisions between two cell populations.

In contrast, collision-induced boundary resistance in C2C12 was not evident in the MDCK–C2C12 pair. The heterotypic boundary was shown to be slowly pushed by the expanding MDCK clusters without much interfacial resistance from C2C12, as evidenced by a gradual increase in traction and maximum shear stress values in C2C12 cells, as opposed to the sharp rises observed in HaCaT–C2C12 collisions. In addition, the variances in both nuclear size and aspect ratio of C2C12 cells were noticeably higher in the HaCaT–C2C12 pair, which may correlate with the collision-induced local alignment of C2C12 cells near the boundary, whereas the C2C12

cells in the MDCK–C2C12 pair were being pushed gently without causing any alterations in nuclear morphology. The apparent differences in the segregation process in the two pairs appeared to stem from the intrinsic differences in homotypic adhesion properties of the constituent cells, their collective migratory behaviors, and the heterotypic collision events at the boundary interface. Although the spatial distributions of maximum shear stress between two pairs, HaCaT–C2C12 and MDCK–C2C12, were dissimilar due to their differential heterotypic contact behavior, they shared the common feature of a local rise in the maximum shear stress at the heterotypic boundary interface. These characteristics in stress distribution may serve as a novel metric for identifying a spatiotemporal phase transition of cells undergoing pathophysiological transitions such as stem cell differentiation or epithelial–mesenchymal transition during wound healing and cancer metastasis.

## MATERIALS AND METHODS

[Request a protocol](#) through *Bio-protocol*.

### Cell culture

The HaCaT (human epidermal keratinocyte) cells, MDCK cells, and C2C12 (mouse myoblast) cells were grown individually in culture media (low-glucose DMEM supplemented with 10% fetal bovine serum [FBS] and 1% penicillin–streptomycin). The cells were kept in an incubator with 5% CO<sub>2</sub> at 37°C.

### Polyacrylamide-gel substrate preparation

Thirty-five millimeter glass-bottom dishes were first prepared by treating the glass surface with bind-silane solutions containing acetic acid, silane A174, and highly purified water with a ratio of 1:2.6:4, respectively. According to the previous protocol (Treat et al., 2009), 2.5 ml of polyacrylamide (PA)-gel solution (3kPa) contained 2042 µl of highly purified water, 344 µl of 40% acrylamide, 112.5 µl of 2% *N,N'*-methylene bis (acrylamide) (BIS) solution, 12.5 µl of 10% ammonium persulfate (APS), 1.3 µl of tetramethylene diamine (TEMED), and 12.5 µl of red fluorescent beads (diameter = 0.5 µm). Each glass-bottom dish was filled with 24 µl of the prepared PA-gel solution, which was then flattened by cover glasses (diameter = 18 mm). To ensure that the fluorescent beads were on the top of the gel, the glass-bottom dishes were centrifuged in an upside-down configuration at 500 rpm for 10 min. The gel was kept at room temperature for another 20 min to allow further polymerization, and the well-spread PA-gel underneath was then coated with a 100 µg/ml collagen I solution (Advanced BioMatrix; PureCol 5005) at 4°C overnight.

### Segregation assays

For segregation assays, HaCaT–C2C12 and MDCK–C2C12 cells were mixed in equal proportions (1:1) with a total density of 600,000 cells/ml (30% confluency) in culture media. Mixed cells were seeded on top of the prepared PA gel. Before time-lapse imaging, samples were kept in the incubator for 6 h to allow the cells to settle and attach to the substrate. Images were taken with a 10× objective lens, using the Axiovert 200M (Carl Zeiss) microscope with the maintenance of incubating condition (5% CO<sub>2</sub> at 37°C). Images were acquired every 10 min for 36 h. To measure the cells' velocity field, stabilized images were analyzed by particle image velocimetry (PIV) software provided by MATLAB. The calculation was based on cross-correlating cell images with an interrogation window size of 64 × 64 pixels and an overlap of 50%. To track the individual migrations of cells, we also analyzed the trajectory patterns of cells during the segregation process. Because the heterotypic cells were intricately

mixed before the segregation, the manual tracking of cells was difficult from the start of imaging. To overcome this problem, first, we marked the epithelial cell types with a cell tracker (CellTracker CMFDA Dye; Invitrogen) and waited for the segregation establishment. Then, the cells were tracked backward from the last images to the initial images. With these steps, we successfully obtained the trajectory of cells during the segregation.

### Measurement of traction force and in-plane stresses of the monolayer

The acquired phase images and fluorescent bead images were pre-processed using ImageJ software and then analyzed using MATLAB source codes provided by J. J. Fredberg's lab at the Harvard T. H. Chan School of Public Health. First, the cells' traction forces were calculated from the displacement of the beads and elastic modulus of the gel using unconstrained Fourier transform traction microscopy (FTTM) (Butler et al., 2002). Next, the intercellular stresses, including the average normal and maximum shear stress values, were calculated using MSM. The calculation was based on the force balance equation using the obtained traction data (Tambe et al., 2011, 2013).

### Alteration of myosin II activity

To investigate the role of actomyosin structures in maintaining the stability of the boundary, we modified actomyosin structures using blebbistatin (Merck; 203389), a myosin II activity inhibitor. After co-cultured cells developed segregation patterns, blebbistatin was treated at a concentration of 50 µM on coculture samples (24 h after seeding). To enhance the myosin activity, we also treated the calyculin A (Sigma-Aldrich; C5552) at a concentration of 2 nM on the coculture samples (24 h after seeding). For focal adhesion inhibition, we used 10 µM FAK Inhibitor 14 (Sigma-Aldrich; SML0937). Then, the drug-treated samples were imaged every 10 min to monitor any changes in the integrity of the boundary.

### Immunostaining

Segregation samples were pretreated with 0.1% Triton X-100 and 3% paraformaldehyde in phosphate-buffered saline (PBS) for 3 min at room temperature and washed once with PBS. Next, samples were fixed with 4% paraformaldehyde for 10 min at room temperature. After fixing the cells, samples were blocked with 3% bovine serum albumin (BSA) for 2 h at room temperature. Next, cells were incubated with the primary antibody at 4°C overnight. After incubation, samples were washed three times with PBS, followed by incubation with secondary antibody for 1 h at room temperature. To stain the actin structure, phalloidin was used to treat the samples for 20 min at room temperature and then with 4',6-diamidino-2-phenylindole (DAPI) for 5 min at room temperature. Finally, all the primary antibodies were diluted in 3% BSA with a ratio of 1:100, secondary antibodies with a ratio of 1:200, and phalloidin with a ratio of 1:50.

### Statistical analysis

Statistical significance was determined by a Mann–Whitney test and one-way analysis of variance (ANOVA) followed by a post-hoc test (Tukey,  $p < 0.05$ ) in Origin software. Statistical significance is marked as \*  $p < 0.05$ , \*\*  $p < 0.01$ , \*\*\*  $p < 0.001$ .

## ACKNOWLEDGMENTS

J. J. Fredberg's lab generously provided TFM and MSM codes at the Harvard T. H. Chan School of Public Health. This work was supported by National Research Foundation of Korea (NRF) grants funded by the Korea government (NRF-2020M3A9E4039658).

## REFERENCES

- Altschuler SJ, Wu LF (2010). Cellular heterogeneity: do differences make a difference? *Cell* 141, 559–563.
- Amack JD, Manning ML (2012). Knowing the boundaries: extending the differential adhesion hypothesis in embryonic cell sorting. *Science* 338, 212–215.
- Beatrice CP, de Almeida RMC, Brunnet LG (2017). Mean-cluster approach indicates cell sorting time scales are determined by collective dynamics. *Phys Rev E* 95, 032402.
- Belmonte JM, Thomas GL, Brunnet LG, de Almeida RMC, Chaté H (2008). Self-propelled particle model for cell-sorting phenomena. *Phys Rev Lett* 100, 248702.
- Brodland GW (2002). The differential interfacial tension hypothesis (DITH): a comprehensive theory for the self-rearrangement of embryonic cells and tissues. *J Biomech Eng* 124, 188–197.
- Burridge K, Wittchen ES (2013). The tension mounts: stress fibers as force-generating mechanotransducers. *J Cell Biol* 200, 9–19.
- Butler JP, Tolić-Nørrelykke IM, Fabry B, Fredberg JJ (2002). Traction fields, moments, and strain energy that cells exert on their surroundings. *Am J Physiol Cell Physiol* 282, C595–C605.
- Canty L, Zarour E, Kashkooli L, François P, Fagotto F (2017). Sorting at embryonic boundaries requires high heterotypic interfacial tension. *Nat Commun* 8, 157.
- Cho Y, Son M, Jeong H, Shin JH (2018). Electric field-induced migration and intercellular stress alignment in a collective epithelial monolayer. *Mol Biol Cell* 29, 2292–2302.
- Fagotto F (2014). The cellular basis of tissue separation. *Development* 141, 3303–3318.
- Fagotto F (2020). Tissue segregation in the early vertebrate embryo. *Semin Cell Dev Biol* 107, 130–146.
- Kabla AJ (2012). Collective cell migration: leadership, invasion and segregation. *J R Soc Interface* 9, 3268–3278.
- Kindberg AA, Srivastava V, Muncie JM, Weaver VM, Gartner ZJ, Bush JO (2021). EPH/EPHRIN regulates cellular organization by actomyosin contractility effects on cell contacts. *J Cell Biol* 220, e202005216.
- Krens SFG, Heisenberg C-P (2011). Cell sorting in development. *Curr Top Dev Biol* 95, 189–213.
- Kwon TY, Jeong J, Park E, Cho Y, Lim D, Ko UH, Shin JH, Choi J (2021). Physical analysis reveals distinct responses of human bronchial epithelial cells to guanidine and isothiazolinone biocides. *Toxicol Appl Pharmacol* 424, 115589.
- Méhes E, Mones E, Németh V, Vicsek T (2012). Collective motion of cells mediates segregation and pattern formation in co-cultures. *PLoS One* 7, e31711.
- Mishra AK, Campanale JP, Mondo JA, Montell DJ (2019). Cell interactions in collective cell migration. *Development* 146, dev172056.
- Notbohm J, Banerjee S, Utuje KJC, Gweon B, Jang H, Park Y, Shin J, Butler JP, Fredberg JJ, Marchetti MC (2016). Cellular contraction and polarization drive collective cellular motion. *Biophys J* 110, 2729–2738.
- O'Neill AK, Kindberg AA, Niethamer TK, Larson AR, Ho HH, Greenberg ME, Bush JO (2016). Unidirectional Eph/ephrin signaling creates a cortical actomyosin differential to drive cell segregation. *J Cell Biol* 215, 217–229.
- Peyret G, Mueller R, d'Alessandro J, Begnaud S, Marcq P, Mège RM, Yeomans JM, Doostmohammadi A, Ladoux B (2019). Sustained oscillations of epithelial cell sheets. *Biophys J* 117, 464–478.
- Salazar-Ciudad I, Jernvall J, Newman SA (2003). Mechanisms of pattern formation in development and evolution. *Development* 130, 2027–2037.
- Schumacher LJ, Maini PK, Baker RE (2017). Semblance of heterogeneity in collective cell migration. *Cell Syst* 5, 119–127.e111.
- Steinberg MS (1970). Does differential adhesion govern self-assembly processes in histogenesis? Equilibrium configurations and the emergence of a hierarchy among populations of embryonic cells. *J Exp Zool* 173, 395–433.
- Steinberg MS (2007). Differential adhesion in morphogenesis: a modern view. *Curr Opin Genet Dev* 17, 281–286.
- Tambe DT, Crouette U, Trepas X, Park CY, Kim JH, Millet E, Butler JP, Fredberg JJ (2013). Monolayer stress microscopy: limitations, artifacts, and accuracy of recovered intercellular stresses. *PLoS One* 8, e55172.
- Tambe DT, Hardin CC, Angelini TE, Rajendran K, Park CY, Serra-Picamal X, Zhou EH, Zaman MH, Butler JP, Weitz DA, et al. (2011). Collective cell guidance by cooperative intercellular forces. *Nat Mater* 10, 469–475.
- Taylor HB, Khuong A, Wu Z, Xu Q, Morley R, Gregory L, Poliakov A, Taylor WR, Wilkinson DG (2017). Cell segregation and border sharpening by Eph receptor-ephrin-mediated heterotypic repulsion. *J R Soc Interface* 14, 20170338.
- Townes PL, Holtfreter J (1955). Directed movements and selective adhesion of embryonic amphibian cells. *J Exp Zool* 128, 53–120.
- Trepas X, Wasserman MR, Angelini TE, Millet E, Weitz DA, Butler JP, Fredberg JJ (2009). Physical forces during collective cell migration. *Nat Phys* 5, 426–430.
- Yang X, Manning ML, Marchetti MC (2014). Aggregation and segregation of confined active particles. *Soft Matter* 10, 6477–6484.